

Directed polymer in a random medium of dimension $1+1$ and $1+3$: weights statistics in the low-temperature phase

Cécile Monthus and Thomas Garel
Service de Physique Théorique, CEA/DSM/SPHT
Unité de recherche associée au CNRS
91191 Gif-sur-Yvette cedex, France

We consider the low-temperature $T < T_c$ disorder-dominated phase of the directed polymer in a random potential in dimension $1+1$ (where $T_c = 1$) and $1+3$ (where $T_c < 1$). To characterize the localization properties of the polymer of length L , we analyse the statistics of the weights $w_L(\mathbf{x})$ of the last monomer as follows. We numerically compute the probability distributions $P_1(w)$ of the maximal weight $w_L^{\max} = \max_{\mathbf{x}} [w_L(\mathbf{x})]$, the probability distribution (Y_2) of the parameter $Y_2(L) = \sum_{\mathbf{x}} w_L^2(\mathbf{x})$ as well as the average values of the higher order moments $Y_k(L) = \sum_{\mathbf{x}} w_L^k(\mathbf{x})$. We find that there exists a temperature $T_{\text{gap}} < T_c$ such that (i) for $T < T_{\text{gap}}$, the distributions $P_1(w)$ and (Y_2) present the characteristic Derrida-Flyvbjerg singularities at $w = 1/n$ and $Y_2 = 1/n$ for $n = 1; 2; \dots$. In particular, there exists a temperature-dependent exponent (T) that governs the main singularities $P_1(w) \sim (1-w)^{-(T)-1}$ and $(Y_2) \sim (1-Y_2)^{-(T)-1}$ as well as the power-law decay of the moments $Y_k(i) \sim 1/k^{(T)}$. The exponent (T) grows from the value $(T=0) = 0$ up to $(T_{\text{gap}}) = 2$. (ii) for $T_{\text{gap}} < T < T_c$, the distribution $P_1(w)$ vanishes at some value $w_0(T) < 1$, and accordingly the moments $Y_k(i)$ decay exponentially as $(w_0(T))^k$ in k . The histograms of spatial correlations also display Derrida-Flyvbjerg singularities for $T < T_{\text{gap}}$. Both below and above T_{gap} , the study of typical and averaged correlations is in full agreement with the droplet scaling theory.

I. INTRODUCTION

A convenient way to characterize disorder-dominated phases is through the statistics of some appropriate "weights". In mean-field models, these weights represent either weights of pure states, as in the replica analysis of the Sherrington-Kirkpatrick model [1], or weights of microscopic configurations, as in the Random Energy Model [2] or in the directed polymer model on the Cayley tree [3]. It turns out that in these three cases, the weights statistics is the same as in Levy sums with some index $0 < \alpha < 1$ [4], where the index α depends on the temperature: for instance in the Random Energy Model [2] or in the directed polymer model on the Cayley tree [3], it is simply $(T) = T/T_c$. In [5], the corresponding probability distributions of the weights were found to exhibit characteristic singularities at some integer inverses. Similar Derrida-Flyvbjerg singularities also occur in many other contexts, such as randomly broken objects [5, 6], in population genetics [7, 8, 9], in random walk excursions or loops [4, 10, 11].

For disordered systems in finite dimensions, it seems appropriate to consider the weights associated to a local degree of freedom, to characterize to what extent it is frozen. To the best of our knowledge, this idea has first been introduced to characterize the freezing of a folded polymer with random self-interactions [12]. It was then used in the context of secondary structures of random RNA to analyse the fraction of frozen pairs between degenerate ground states [13], and to characterize the freezing transition [14].

In this paper, we study the statistics of the weights $w_L(\mathbf{x})$ of the end-point of a directed polymer in a random potential [15]. We focus here on the low-temperature $T < T_c$ disorder-dominated phase both in dimension $1+1$ (where $T_c = 1$) and $1+3$ (where $T_c < 1$), since we have studied elsewhere [16] the weights statistics at criticality in $d = 3$, where multifractal behavior occurs. We are not aware of previous studies on these weights in the physics literature. On the contrary, in the mathematical literature, the weight of the favourite site has been considered as a localization criterion [17, 18], and a more detailed description of end-point weights was then given via the notion of atoms [19].

The paper is organized as follows. The model and observables are introduced in Section II. We then present a detailed study of the weights of the end-point of the directed polymer both in dimensions $1+1$ and $1+3$. For clarity, the statistical properties of the weights alone, independently of the distances involved are described in Section III, whereas the study of spatial properties is postponed to Section IV. We summarize our results in Section V.

II. MODEL AND OBSERVABLES

A. Model definition

In this paper, we present numerical results for the random bond version of the model defined by the recursion relation on a cubic lattice in $d = 1$ and $d = 3$

$$Z_{t+1}(\mathbf{r}) = \prod_{j=1}^d e^{-\epsilon_t(\mathbf{r} + \mathbf{e}_j; \mathbf{r})} Z_t(\mathbf{r} + \mathbf{e}_j) \quad (1)$$

The bond energies $\epsilon_t(\mathbf{r} + \mathbf{e}_j; \mathbf{r})$ are random independent variables drawn from the Gaussian distribution

$$P(\epsilon) = \frac{1}{\sqrt{2\pi}} e^{-\frac{\epsilon^2}{2}} \quad (2)$$

In this paper, we consider the following boundary conditions. The first monomer is fixed at $\mathbf{r} = \mathbf{0}$, i.e. the initial condition of the recurrence of Eq. (1) reads

$$Z_{t=0}(\mathbf{r}) = \delta_{\mathbf{r}, \mathbf{0}} \quad (3)$$

The last monomer is free, i.e. the full partition function of the polymer of length L is then obtained by summing over all possible positions \mathbf{r} at $t = L$

$$Z_L^{\text{tot}} = \sum_{\mathbf{r}} Z_L(\mathbf{r}) \quad (4)$$

This model has attracted a lot of attention because it is directly related to non-equilibrium properties of growth models [15]. Within the field of disordered systems, it is also very interesting on its own because it represents a ‘baby-spin-glass’ model [3, 4, 15, 20, 21]. At low temperature, there exists a disorder dominated phase, where the order parameter is an ‘overlap’. In finite dimensions, a scaling droplet theory was proposed [21, 22], in direct correspondence with the droplet theory of spin-glasses [23], whereas in the mean-field version of the model on the Cayley, a freezing transition very similar to the one occurring in the Random Energy Model was found [3]. The phase diagram as a function of space dimension d is the following [15]. In dimension $d \leq 2$, there is no free phase, i.e. any initial disorder drives the polymer into the strong disorder phase, whereas for $d > 2$, there exists a phase transition between the low temperature disorder dominated phase and a free phase at high temperature [24, 25].

In the following, we will focus on the statistical properties of the weights

$$w_L(\mathbf{r}) = \frac{Z_L(\mathbf{r})}{Z_L^{\text{tot}}} \quad (5)$$

normalized to (Eq. 4)

$$\sum_{\mathbf{r}} w_L(\mathbf{r}) = 1 \quad (6)$$

The numerical results given below have been obtained using polymers of various lengths L , with corresponding numbers $n_s(L)$ of disordered samples with the values

$$L = 50; 100; 200; 400; 800 \quad (7)$$

$$n_s(L) = 13 \cdot 10^7; 35 \cdot 10^6; 9 \cdot 10^6; 225 \cdot 10^4; 57 \cdot 10^4 \quad (8)$$

in $d = 1$, and the values

$$L = 6; 12; 18; 24; 36; 48; 60 \quad (9)$$

$$n_s(L) = 10^8; 10^7; 2 \cdot 10^6; 8 \cdot 10^5; 2 \cdot 10^5; 5 \cdot 10^4; 3 \cdot 10^4 \quad (10)$$

in $d = 3$. In the following, \overline{A} denotes the average of A over the disorder samples.

B. Characterization of the weights statistics

In analogy with the weight statistics in Levy sums and in the Random Energy Model [4, 5], we have numerically computed the probability distribution $P_1(w)$ of the maximal weight (Eq. 5)

$$w_L^{\max} = \max_{\mathbf{x}} f w_L(\mathbf{x}) g \quad (11)$$

as well as the probability distribution $P_2(w)$ of the second maximal weight. Another useful way to characterize the statistical properties of the weights [4, 5] is to consider the moments of arbitrary order k

$$Y_k(L) = \sum_{\mathbf{x}} w_L^k(\mathbf{x}) \quad (12)$$

which represents the probability that the last monomer of the polymer of length L is at the same point in k different thermal configurations of the same disordered sample. We have measured the probability Y_2 of the parameter

$$Y_2(L) = \sum_{\mathbf{x}} w_L^2(\mathbf{x}) \quad (13)$$

as well as the moments $\overline{Y_k(L)}$ for $2 \leq k \leq 100$. Finally, we have also computed the weights density

$$f_L(w) = \sum_{\mathbf{x}} \delta(w - w_L(\mathbf{x})) \quad (14)$$

giving rise to the moments

$$\overline{Y_k(L)} = \int_0^1 dw w^k f_L(w) \quad (15)$$

The normalization condition for the density $f_L(w)$ is

$$\overline{Y_1(L)} = \int_0^1 dw w f_L(w) = 1 \quad (16)$$

In the following, we will also present histograms of the associated entropy

$$S_L = - \sum_{\mathbf{x}} w_L(\mathbf{x}) \ln w_L(\mathbf{x}) \quad (17)$$

III. STUDY OF THE WEIGHTS STATISTICS

A. Probability distribution $P_1(w)$ of the largest weight

The probability distributions $P_1(w)$ and $P_2(w)$ of the largest (Eq. 11) and second largest weights of the last monomer in dimension $1 + 1$ are shown on Fig. 1 for two temperatures. These curves show that there exists a temperature $T_{\text{gap}} (d=1) \approx 0.7$ such that

(i) for $T < T_{\text{gap}}$ (see Fig. 1 a) the distribution $P_1(w)$ reaches the point $w = 1$ with a singularity parametrized by a temperature-dependent exponent

$$P_1(w) \sim (1 - w)^{(T) - 1} \quad (18)$$

Beyond this main singularity, $P_1(w)$ also presents characteristic Derrida-Flyvbjerg singularities at $w = 1/2, 1/3, \dots, 1/n, \dots$ [5]: in particular, the singularity of $P_1(w)$ at $w = 1/2$ is clearly visible on Fig. 1 a. Similarly, the distribution $P_2(w)$ reaches the point $w = 1/2$ (see Fig. 1 a)

(ii) for $T > T_{\text{gap}}$ (see Fig. 1 b) the distribution $P_1(w)$ does not reach $w = 1$ anymore, but vanishes at some maximal value $0 < w_0(T) < 1$

$$P_1(w) \sim (w_0(T) - w) \quad (19)$$

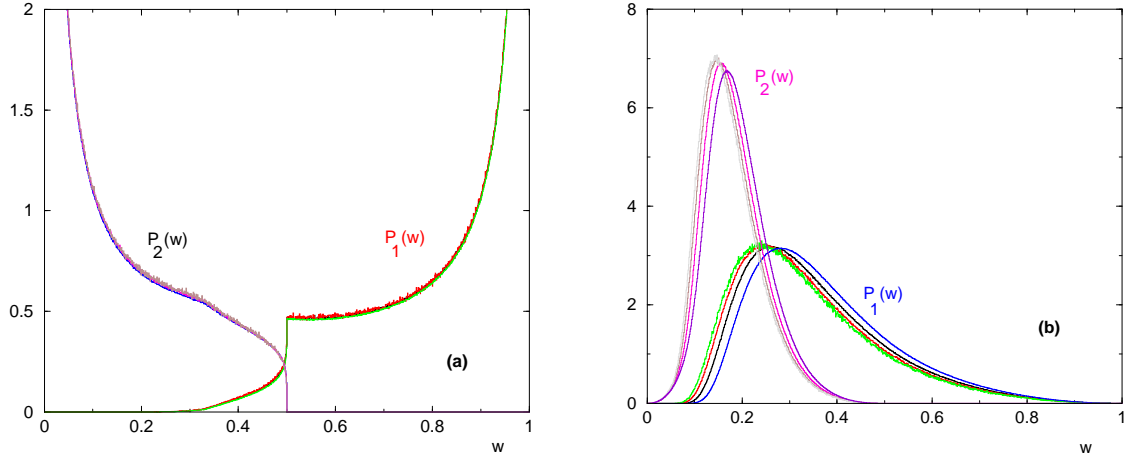


FIG. 1: (Color online) $d = 1$: Probability distributions $P_1(w)$ and $P_2(w)$ of the largest and second largest weight seen by the last monomer (see Eq. 11) (a) at $T = 0.1$ ($T < T_{\text{gap}}$) for $L = 50; 100; 200$: the characteristic Derrida-Flyvbjerg singularities at $w = 1$ and $w = 1/2$ are clearly visible. (b) at $T = 1$: ($T > T_{\text{gap}}$) for $L = 50; 100; 200; 400$: the distribution $P_1(w)$ does not reach $w = 1$ anymore, and the distribution $P_2(w)$ does not reach $w = 1/2$ anymore.

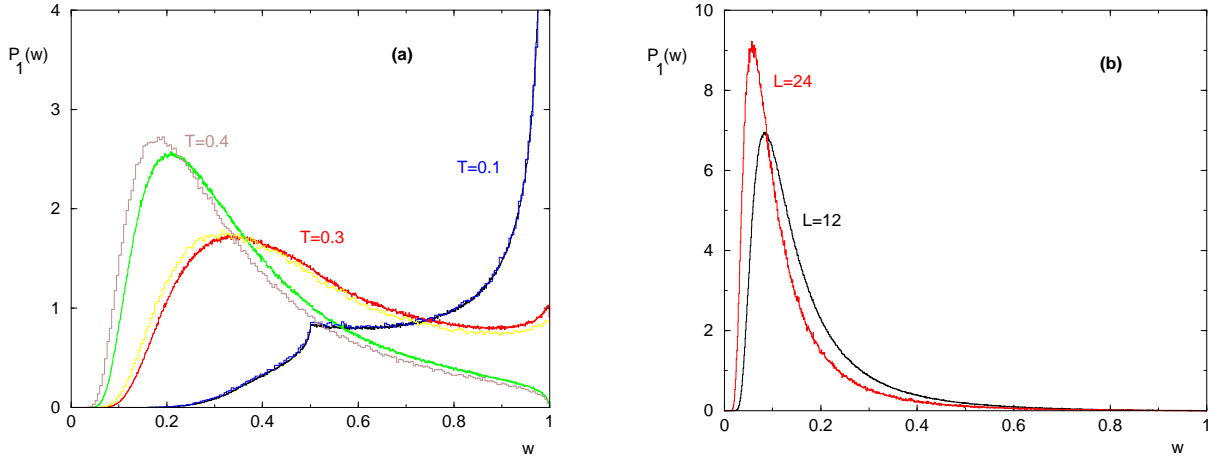


FIG. 2: (Color online) $d = 3$: Probability distribution $P_1(w)$ of the largest weight seen by the last monomer (see Eq. 11) (a) at $T = 0.1$ ($T < 1$), $T = 0.3$ ($T < 1$), $T = 0.4$ ($1 < T < 2$) for $L = 12; 24$. (b) at $T = 0.6 > T_{\text{gap}}$ for $L = 12; 24$.

with some exponent α . Similarly, the distribution $P_2(w)$ does not reach the point $w = 1/2$ (see Fig. 1 b).

This temperature T_{gap} in $1+1$ where $T_c = 1$ also exists in $1+3$ where T_c is finite, as shown on Fig. 2. On Fig. 2 a, the distribution $P_1(w)$ is shown for three temperatures below T_{gap} with exponents $(T = 0.1) < 1$, $(T = 0.3) = 1$ and $1 < (T = 0.4) < 2$. On Fig. 2 b, the distribution $P_1(w)$ is shown for temperature $T = 0.6$ in the region $T_{\text{gap}} (d=3) < 0.5 < T < T_c = 0.79$.

Note that here we only describe the low-temperature phase $T < T_c$ and we refer to [16] for a detailed study of the weights statistics at criticality $T_c = 0.79$ where multifractal behavior occurs.

$$B. \quad \text{Probability distribution } G_L(s) \text{ of the entropy } s_L = -\sum_{\mathbf{x}} w_L(\mathbf{x}) \ln w_L(\mathbf{x})$$

The Derrida-Flyvbjerg singularities found for $T < T_{\text{gap}}$ at $w = 1/n$ for the weights translate into singularities in the histograms of the last-monomer entropy (Eq. 17) at $s = 0; \ln 2; \ln 3; \dots$. In particular, the main singularity of $P_1(w)$ for $w \neq 1$ (Eq. 18) yields a corresponding singularity at $s \neq 0$

$$G(s) \sim s^{-(T)-1} \quad (20)$$

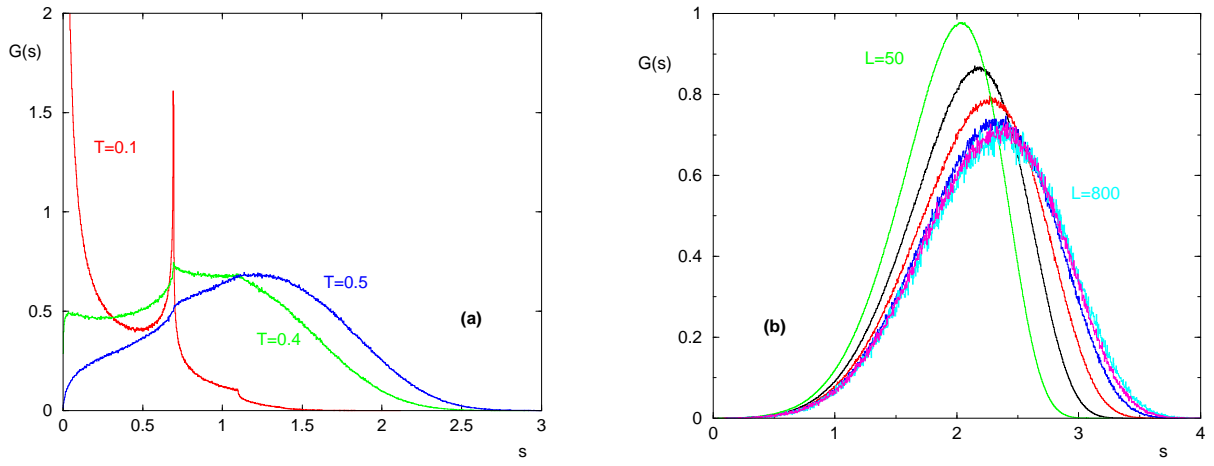


FIG. 3: (Color online) $d = 1$: Probability distribution $G_L(s)$ of the last monomer entropy $s_L = -\sum_{\mathbf{x}} w_L(\mathbf{x}) \ln w_L(\mathbf{x})$ (a) at three temperatures below T_{gap} namely $T = 0.1$ ($0 < 1$), $T = 0.4$ ($0 < 1$), $T = 0.5$ ($1 < 2$) for $L = 200$: the Derrida-Flyvbjerg singularities at $s = 0$, $s = \ln 2$ and $s = \ln 3$ are clearly visible. (b) at $T = 1 > T_{\text{gap}}$ for $L = 50; 100; 200; 400; 600; 800$: the histogram does not reach $s = 0$.

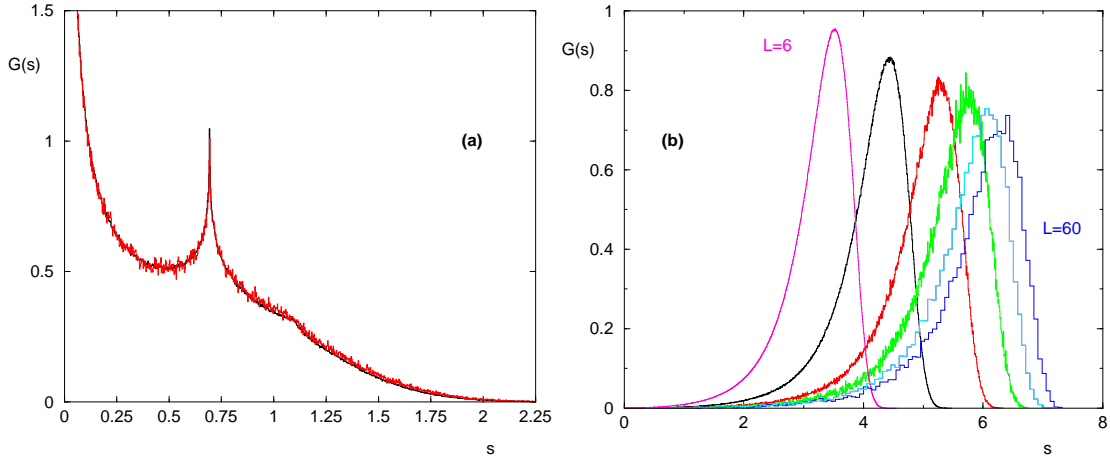


FIG. 4: (Color online) $d = 3$ Probability distribution $G_L(s)$ of the last monomer entropy $s_L = -\sum_{\mathbf{x}} w_L(\mathbf{x}) \ln w_L(\mathbf{x})$ (a) at $T = 0.1 < T_{\text{gap}}$ for $L = 12; 24$: the Derrida-Flyvbjerg singularities at $s = 0$, $s = \ln 2$ and $s = \ln 3$ are clearly visible. (b) at $T = 0.6 > T_{\text{gap}}$ for $L = 6; 12; 24; 36; 48; 60$: the histogram does not reach $s = 0$.

for $0 < T < T_{\text{gap}}$, whereas a gap s_{min} appears for $T > T_{\text{gap}}$. This is shown on Fig. 3 for $d = 1$ and on Fig. 4 for $d = 3$.

C . Probability distribution $\Pi(Y_2)$ of the parameter Y_2

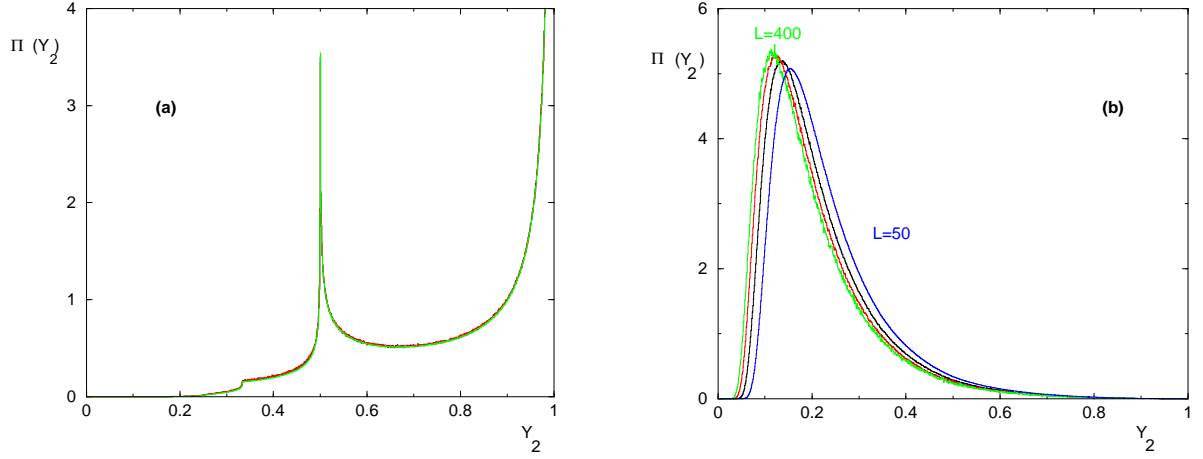


FIG. 5: (Color online) $d = 1$: Probability distribution $\Pi(Y_2)$ of the parameter $Y_2 = \sum_{\mathbf{x}} w_L^2(\mathbf{x})$ (a) at $T = 0.1 < T_{\text{gap}}$ for $L = 50; 100; 200$: the Derrida-Flyvbjerg singularities at $Y_2 = 1, Y_2 = 1/2$ and $Y_2 = 1/3$ are clearly visible. (b) at $T = 1 > T_{\text{gap}}$ for $L = 50; 100; 200; 400$: the histogram does not reach $Y_2 = 1$.

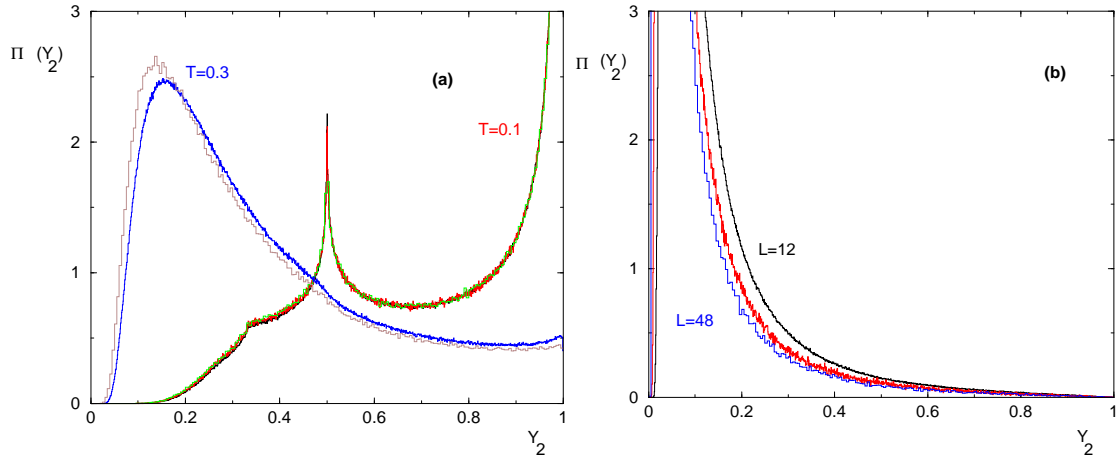


FIG. 6: (Color online) $d = 3$: Probability distribution $\Pi(Y_2)$ of the parameter $Y_2 = \sum_{\mathbf{x}} w_L^2(\mathbf{x})$ (a) for $T = 0.1$ ($L = 12; 18; 24$) and $T = 0.3$ ($L = 12; 24$) : the Derrida-Flyvbjerg singularities at $Y_2 = 1, Y_2 = 1/2$ and $Y_2 = 1/3$ are clearly visible. (b) for $T = 0.5 > T_{\text{gap}}$ with $L = 12; 24; 48$

The parameter Y_2 defined in Eq. 13 can reach the value $Y_2 = 1$ only if the maximal weight w^{max} also reaches $w^{\text{max}} = 1$. As a consequence, the probability distribution $\Pi(Y_2)$ has the same singularity near $Y_2 = 1$ as in Eq. (18)

$$\Pi(Y_2) \sim (1 - Y_2)^{(T)-1} \quad (21)$$

for $0 < T < T_{\text{gap}}$. Beyond this main singularity, the distribution $\Pi(Y_2)$ presents the characteristic Derrida-Flyvbjerg singularities at $Y_2 = 1/n$ as shown on Fig. 5 a for $d = 1$ and on Fig. 6 a for $d = 3$. Again for $T > T_{\text{gap}}$, a gap appears as shown on Fig. 5 b for $d = 1$ and on Fig. 6 b for $d = 3$.

D . Density $f(w)$

The density $f(w)$ introduced in Eq. (14) is shown on Fig. 7 and Fig. 8 for $d = 1$ and $d = 3$ respectively.

By construction, this density coincides with the maximal weight distribution $P_1(w)$ for $w > 1/2$, with the sum $(P_1(w) + P_2(w))$ of the two largest weight distributions for $1/3 < w < 1/2$, and so on [5]. As a consequence, $f(w)$

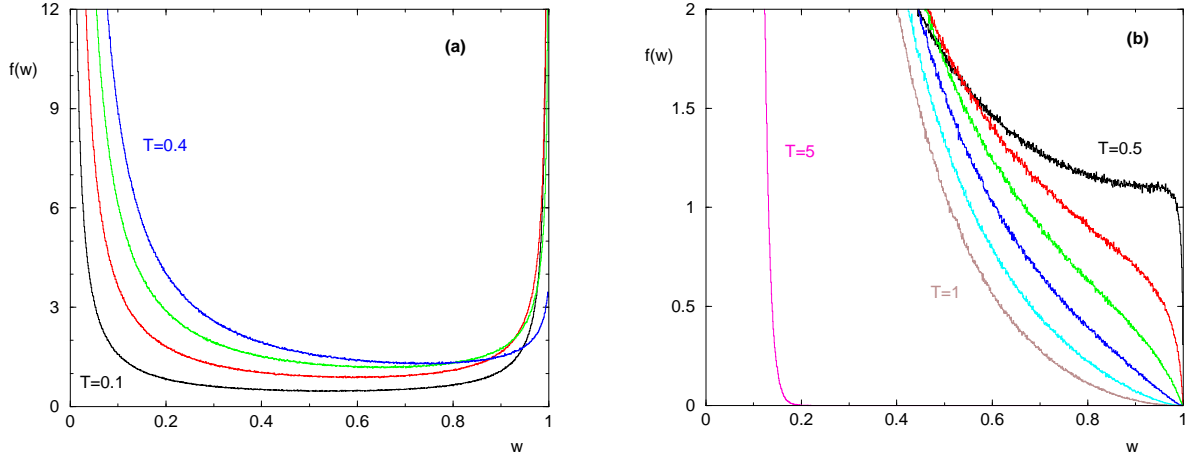


FIG. 7: (Color online) $d = 1$: Weight density $f(w)$ (a) at $T = 0.1; 0.2; 0.3; 0.4$ where $(T) < 1$ for $L = 200$: the weight density $f(w)$ diverges at $w \rightarrow 0$ and $w \rightarrow 1$. (b) at $T = 0.5; 0.6; 0.7; 0.8; 0.9; 1; 5$: for $L = 200$: these curves show the temperature dependent singularity at $w = 1$.

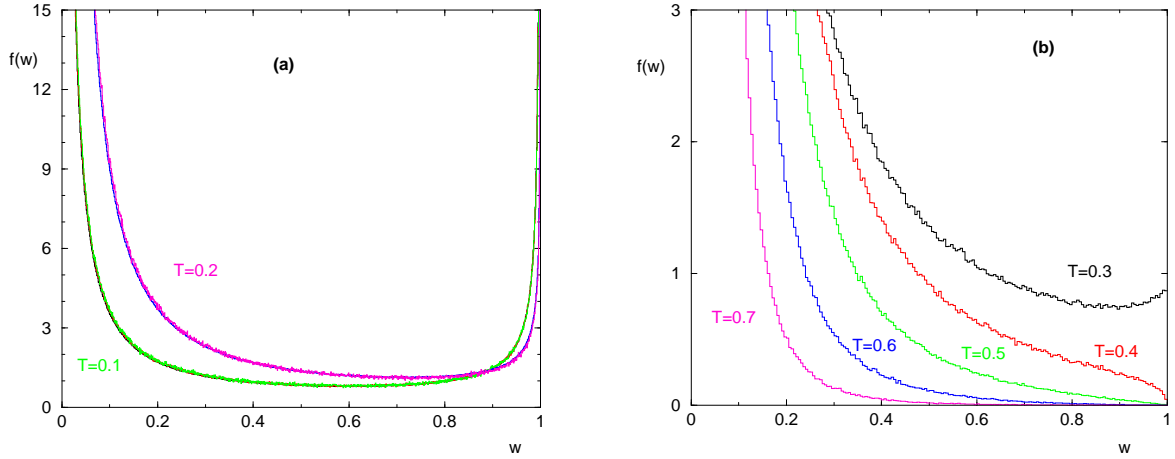


FIG. 8: (Color online) $d = 3$: Weight density $f(w)$ (a) for $T = 0.1$ ($L = 12; 18; 24$) and $T = 0.2$ ($L = 12; 24$) where $(T) < 1$: the weight density $f(w)$ diverges at $w \rightarrow 0$ and $w \rightarrow 1$. (b) for $T = 0.3; 0.4; 0.5; 0.6; 0.7$ ($L = 24$): these curves show that the gap appears around $T_{\text{gap}}(d=3) \approx 0.5$.

has the same singularity near $w \rightarrow 1$ as $P_1(w)$ (Eq. 18), and the same gap (Eq. 19) as long as $w_0(T) > 1/2$. The only other singularity is near $w \rightarrow 0$ where $f(w)$ diverges in a non-integrable manner, because in the $L \rightarrow 1$, there is an infinite number of vanishing weights (only the product $(wf(w))$ has to be integrable at $w = 0$ as a consequence of the normalization condition of Eq. 16).

E. Moments $\overline{Y_k}$

For $0 < T < T_{\text{gap}}$, where $P_1(w)$ and $f(w)$ behaves near $w \rightarrow 1$ as in Eq. 18, the decay in k of the averaged moments $\overline{Y_k(i)}$ (Eq. 12) follow a power-law of exponent (T)

$$\overline{Y_k(i)} \sim \frac{1}{k^{(T)}} \quad \text{for } T < T_{\text{gap}} \quad (22)$$

The behavior of $\overline{Y_k}$ for $k \rightarrow 100$ are shown on Fig. 9 a for $d=1$ and Fig. 10 a for $d=3$. The corresponding exponent (T) are shown on Fig. 9 b for $d=1$ and Fig. 10 b for $d=3$.

For $T > T_{\text{gap}}$ where there exists a gap $w_0(T)$ for $P_1(w)$, the behavior of Eq. 19 also applies to $f(w)$ as long as

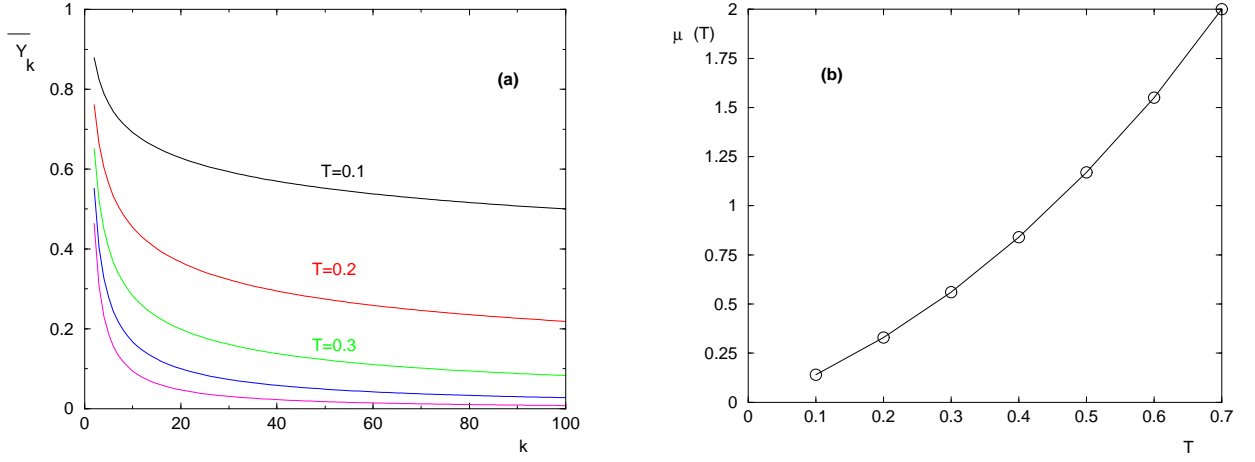


FIG. 9: (Color online) $d = 1$: (a) Decay of the moments \overline{Y}_k of Eq. 22 as a function of k 100 for $L = 800$ and $T = 0.1; 0.2; 0.3; 0.4; 0.5$ (b) Exponent $\mu(T)$ as measured from the slope of the log-log decay in the asymptotic region.

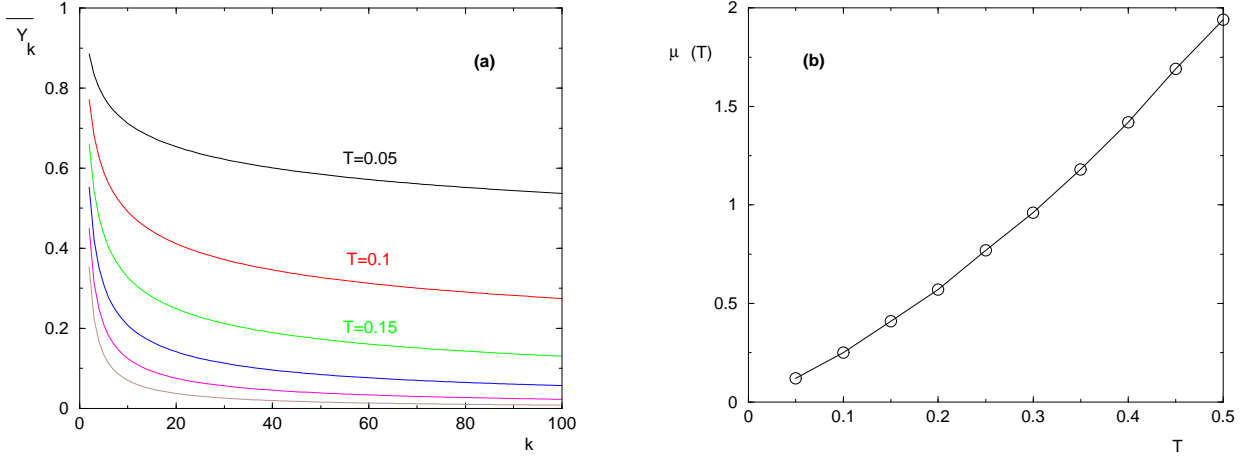


FIG. 10: (Color online) $d = 3$: (a) Decay of the moments \overline{Y}_k of Eq. 22 as a function of k 100 for $L = 48$ and $T = 0.05; 0.1; 0.15; 0.2; 0.25; 0.3$ (b) Exponent $\mu(T)$ as measured from the slope of the log-log decay in the asymptotic region.

$w_0(T) > 1=2$ (since $f(w) = P_1(w)$ for $w > 1=2$ as mentioned above) and thus the decay is then exponential

$$\overline{Y}_k(i) / k! \sim \frac{(w_0(T))^k}{k^{1+}} \quad \text{for } T > T_{\text{gap}} \quad (23)$$

IV. STUDY OF SPATIAL PROPERTIES

In the previous Section, we have studied in details the statistics of the weights independently of their spatial organization. In this section, we study the statistics of the transverse spatial correlation

$$C(r) = \langle w(\mathbf{r}_{\text{pref}}) w(\mathbf{r}_{\text{pref}} + \mathbf{r}) \rangle \quad (24)$$

centered on the preferred position \mathbf{r}_{pref} of maximal weight (Eq. 11). We first recall the predictions of the droplet scaling analysis [21, 22] that will be useful to analyse our numerical results.

A. Reminder on the droplet scaling analysis

The droplet theory for directed polymers [21, 22], is very similar to the droplet theory of spin glasses [23]. It is a scaling theory that can be summarized as follows.

1. Statistics of low energy excitations above the ground state

At very low temperature $T \rightarrow 0$, all observables are governed by the statistics of low energy excitations above the ground state. An excitation of large length l costs a random energy

$$E(l) = l^u \quad (25)$$

where u is a positive random variable distributed with some law $Q_0(u)$ having some finite density at the origin $Q_0(u=0) > 0$. The exponent u is the exponent governing the fluctuation of the energy of the ground state is exactly known in one-dimension ($d=1$) $= 1/3$ [26, 27, 28, 29] and for the mean-field version on the Cayley tree ($d=1$) $= 0$ [3]. In finite dimensions $d=2;3;4;5;\dots$, the exponent $u(d)$ has been numerically measured, and we only quote here the results of the most precise study we are aware of [30] for dimensions $d=2;3$: $u(d=2) = 0.244$ and $u(d=3) = 0.186$.

From (25), the probability distribution of large excitations $l \gg 1$ reads within the droplet theory

$$dl(E=0;l) = \frac{dl}{l} e^{-E(l)} = \frac{dl}{l} e^{-l^u} \quad (26)$$

where the factor $dl=l$ comes from the notion of independent excitations [23]. In particular, its average over the disorder follows the power-law

$$\overline{dl(E=0;l)} = \int_0^{Z+1} du Q_0(u) \frac{dl}{l} e^{-l^u} = T Q_0(0) \frac{dl}{l^{1+}} \quad (27)$$

This prediction describes very well the numerical data in the regime $1 \ll l \ll L$ in dimensions $d=1;2;3$ [31].

Since correlation functions at large distance are directly related to the probability of large excitations, we already see that the low temperature phase is very non-trivial from the point of view of correlations lengths: the typical exponential decay (26) indicates a finite typical correlation length $\xi_{\text{typ}}(T)$, whereas the averaged power-law behavior (27) means that the averaged correlation length $\xi_{\text{av}}(T)$ is actually infinite in the whole low temperature phase

$$\xi_{\text{av}}(0 < T < T_c) = \infty \quad (28)$$

Note that within the droplet theory of spin-glasses [23], the correlation length $\xi_{\text{av}}(T)$ is also infinite in the whole low temperature phase for the same reasons.

2. Low temperature phase governed by a zero-temperature fixed point

According to the droplet scaling theory [21, 22] the whole low temperature phase $0 < T < T_c$ is governed by a zero-temperature fixed point. However, many subtleties arise because the temperature is actually 'dangerously irrelevant'. The main conclusions of the droplet analysis [21, 22] can be summarized as follows. The scaling (25) governs the free energy cost of an excitation of length l , provided one introduces a longitudinal correlation length $\xi_{\parallel}(T)$ to rescale the length l

$$F(l) = \frac{1}{\xi_{\parallel}(T)} l^u \quad (29)$$

Here as before, u denotes a positive random variable distributed with some law $Q(u)$ having some finite density at the origin $Q(u=0) > 0$. As a consequence, the probability of a droplet of size $l \gg 1$ follows the scaling form

$$dl(l) = \frac{dl}{l} e^{-\frac{l}{\xi_{\parallel}(T)}} \quad (30)$$

In particular, the typical behavior follows an exponential decay with exponent

$$\overline{\ln(l)} = \frac{1}{\xi_{\parallel}(T)} \int_0^{Z+1} du u Q(u) \quad (31)$$

whereas the average over the disorder follows the power-law

$$\overline{dl(l)} = Q(0) \frac{dl}{l} \frac{\xi_{\parallel}(T)}{l} \quad (32)$$

This average is governed by the rare events having $u \rightarrow 0$.

A droplet of longitudinal size l corresponds a transverse distance $r \sim l$, where

$$r = \frac{1 + \nu}{2} l \quad (33)$$

ν is the roughness exponent of the low temperature phase [15]. Via the change of variable $r \sim l$, the droplet distribution of Eq. 30 translates into the following scaling form for the correlation at large distance r [21, 22]

$$r^{d-1} C(r) = dl(l) = \frac{dr}{r} e^{-u\left(\frac{r}{\xi(T)}\right)} \quad (34)$$

where the transverse correlation length reads $\xi(T) = [\xi(T)]$, i.e. nally

$$C(r) = \frac{1}{r^d} e^{-u\left(\frac{r}{\xi(T)}\right)} \quad (35)$$

As a consequence, the typical behavior follows an exponential decay with exponent u

$$\overline{\ln C(r)} = -\frac{r}{\xi(T)} \quad d \ln r \quad (36)$$

whereas the average over the disorder is governed by the rare events and follows the power-law

$$\overline{C(r)} = \frac{1}{r^d} \left(\frac{\xi(T)}{r} \right)^{-u} \quad (37)$$

We now describe our numerical data and compare with these predictions.

B. Disorder averaged correlation $\overline{C_L(r)}$

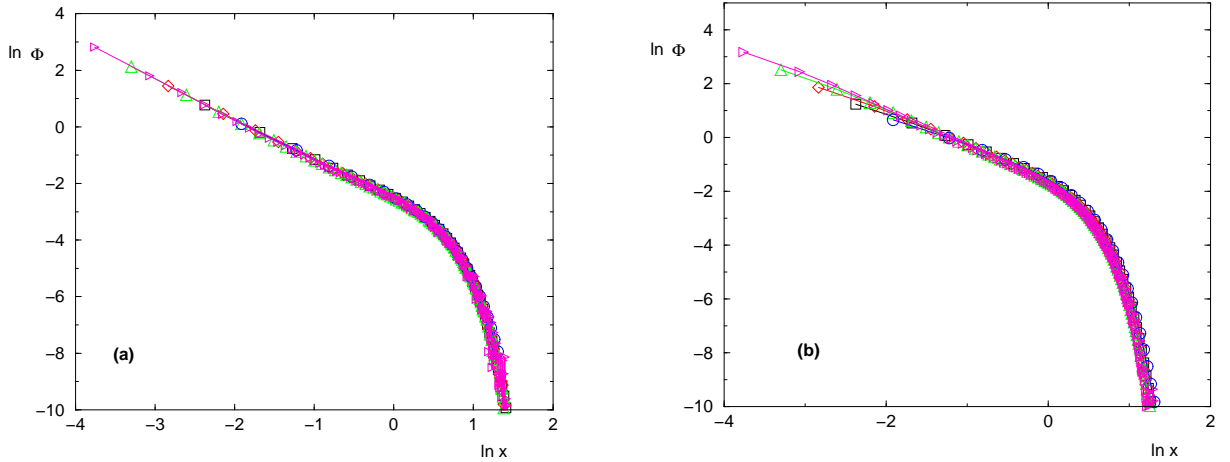


FIG. 11: (Color online) Disorder averaged correlation $\overline{C_L(r)}$ in $d = 1$: finite-size scaling of (Eq. 38): $\ln \Phi = \ln(L \overline{C_L(r)})$ as a function of $\ln x = \ln(r L^{2/3})$ for $L = 50$ (); 100 (); 200 (); 400 (); 800 (B) (a) for $T = 0.2 < T_{\text{gap}}$ (b) for $T = 1 > T_{\text{gap}}$

The previous predictions concern the limit $L \rightarrow \infty$. To compare with our numerical data, we now recall the corresponding finite-size behaviors within the droplet theory [22]. The power-law behavior (Eq. 37) for the averaged correlation translates into the following scaling form for finite L

$$\overline{C_L(r)} = \frac{1}{L^{d+u}} x = \frac{r}{L} \quad (38)$$

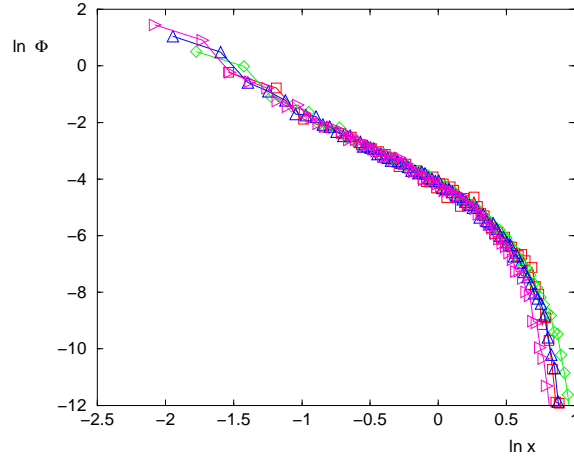


FIG. 12: (Color online) $d = 3$: Disorder averaged correlation $\overline{C_L(r)}$ in $d = 3$ finite-size scaling of (Eq. 38) : (Eq. 38) : $\ln \Phi = \ln(L^{d+1} \overline{C_L(r)})$ as a function of $\ln x = \ln(r=L)$ for $T = 0.1$ $L = 24$ (); 36 (); 48 (4); 60 (B) .

where the scaling function $\Phi(v)$ behaves as the following power-law

$$\Phi(v) \sim \frac{1}{v^{d+1}} \quad (39)$$

to recover Eq. 37 as $L \rightarrow \infty$.

We show on Fig. 11 the finite-size scaling analysis of Eq. 38 in $d = 1$ for two temperatures, one below and one above T_{gap} . In both cases, the agreement with the droplet scaling ansatz is very good, confirming the zero-temperature fixed point picture. The corresponding finite-size scaling analysis for the disorder averaged correlation in $d = 3$ is shown on Fig. 12.

C. Typical correlation $\overline{\ln C_L(r)}$

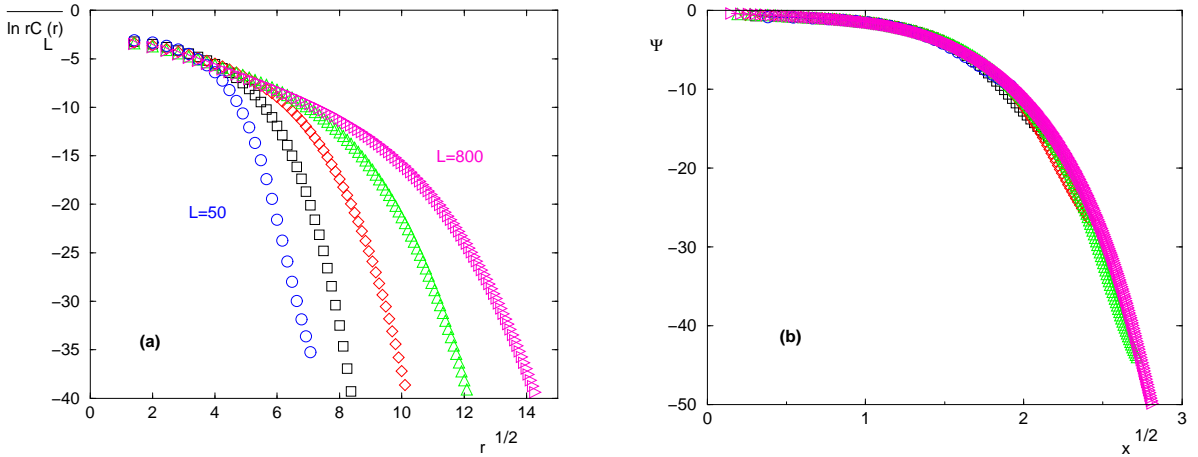


FIG. 13: (Color online) Typical correlation $\overline{\ln C_L(r)}$ in $d = 1$ for $T = 1$ and sizes $L = 50$ (); 100 (); 200 (); 400 (4); 800 (B) : (a) $(\ln C_L(r) + \ln(r))$ as a function of $r^{1/2}$ (see Eq. 36) (b) finite-size scaling of the same data : $\Psi = (\ln C_L(r) + \ln(r))L^{1/2}$ as a function of $x^{1/2} = (r=L^{2/3})^{1/2}$ (see Eq. 40).

The typical correlation of Eq. 36 are shown on Fig. 13 a for $d = 1$ and on Fig. 14 a for $d = 3$ respectively : the collapse for small r is satisfactory. To take into account the L dependent cut-off for large r , we have tried the following finite-size scaling form

$$\overline{\ln C_L(r) + d \ln r} \sim L \quad x = \frac{r}{L} \quad (40)$$

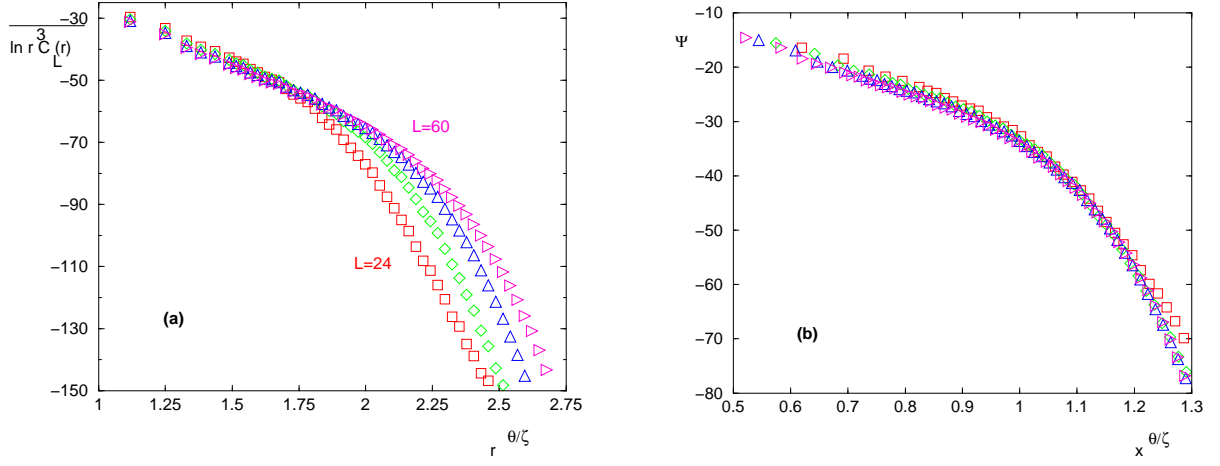


FIG. 14: (Color online) Typical correlation $\ln C_L(r)$ in $d = 3$ for $T = 0.1$ and sizes $L = 24$ (); 36 (); 48 (); 60 (). (a) $(\ln C_L(r) + d \ln(r))$ as a function of $r = r_0 \cdot 3^{1/4}$ (see Eq. 36) (b) finite-size scaling of the same data : $(\ln C_L(r) + d \ln(r)) = L \psi$ as a function of $x = (r-L)/L$ (see Eq. 40) .

where the scaling function $\psi(v)$ behaves as the following power-law

$$\psi(v) \sim v^{-\alpha} \quad (41)$$

to recover Eq. 36 as $L \rightarrow \infty$.

The results for $d = 1$ and $d = 3$ are shown on Fig. 13 b and 14 b respectively.

D. Histograms of correlation function

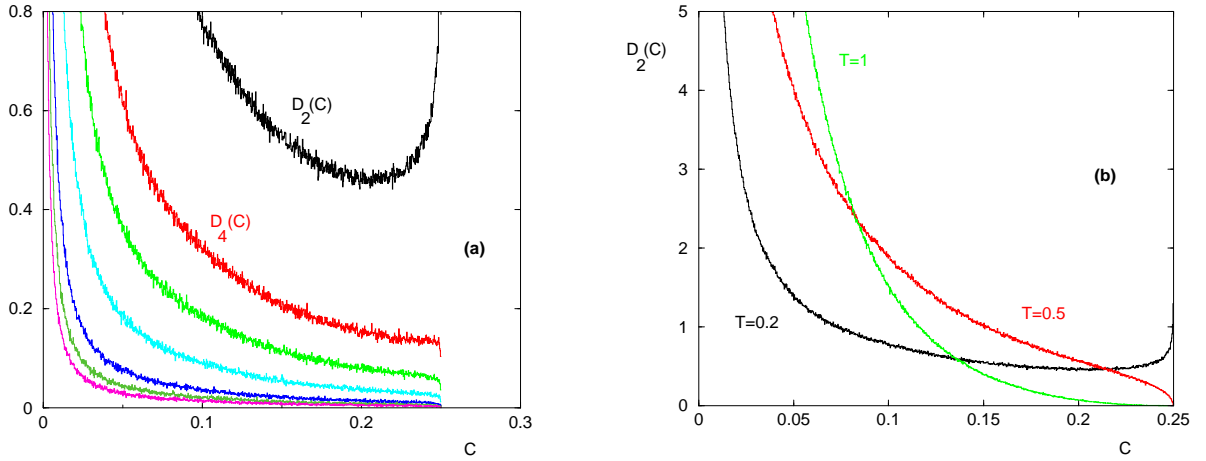


FIG. 15: (Color online) $d = 1$: Probability distribution $D_r(C)$ of the correlation $C(r)$ (Eq. 24) for $L = 200$ (a) for $T = 0.2 < T_{\text{gap}}$ the distribution $D_r(C)$ reaches the maximal value $C_{\text{max}} = 1/4$ for any distance r : here $r = 2; 4; 6; 10; 20; 30; 40$ (b) Probability distribution $D_{r=2}(C)$ of the correlation of two neighboring sites for $T = 0.2$ where $(T) < 1$, $T = 0.5$ where $1 < (T) < 2$ and $T = 1$: $> T_{\text{gap}}$ where the histogram does not reach the maximal possible value $C_{\text{max}} = 1/4$.

Since typical and disorder averaged correlations are very different, we have also studied in $d = 1$ the probability distribution $D_r(C)$ of the correlation $C(r)$ (Eq. 24) between the preferred position and a site at transverse distance r . For $T < T_{\text{gap}}$, the distribution $D_r(C)$ reaches the maximal possible value $C_{\text{max}} = 1/4$ for any distance r as shown on Fig. 15 a. This maximal value $C_{\text{max}} = 1/4$ corresponds to the case where the maximal weight and second maximal weight are both of order $w_1 = 2$ and are at distance r . For large r $L^{2/3}$, this corresponds to the droplet excitations.

For $T > T_{\text{gap}}$, the distribution $D_r(C)$ does not reach the maximum possible value $C_{\text{max}} = 1/4$ anymore, as shown on Fig. 15 b.

V. CONCLUSION

We have studied the weight statistics in the low-temperature $T < T_c$ disorder-dominated phase of the directed polymer in a random potential in dimension $1+1$ (where $T_c = 1$) and $1+3$ (where $T_c < 1$). In particular, we have found a temperature $T_{\text{gap}} < T_c$ with the following properties. For $T < T_{\text{gap}}$, the histograms of weight observables and of spatial correlation display characteristic Derrida-Flyvbjerg singularities. In particular, there exists a temperature-dependent exponent $\gamma(T)$ that governs the main singularities of $P_1(w) \sim (1-w)^{\gamma(T)-1}$, $\langle Y_2 \rangle \sim (1-\gamma)^{\gamma(T)-1}$ and $G(s) \sim s^{\gamma(T)-1}$, as well as the power-law decay of the moments $Y_k(i) \sim k^{-\gamma(T)}$. The exponent $\gamma(T)$ grows from the value $\gamma(T=0) = 0$ up to $\gamma(T_{\text{gap}}) = 2$. For $T_{\text{gap}} < T < T_c$, the distribution $P_1(w)$ vanishes at some value $w_0(T) < 1$, and accordingly the moments $Y_k(i)$ decay exponentially as $(w_0(T))^k$ in k . Finally, our numerical results concerning typical and averaged correlations are in full agreement with the droplet scaling theory both below and above T_{gap} .

Together with our previous study on the freezing transition of random RNA secondary structures [14], this shows that the weight statistics is an efficient tool to characterize to which extent local degrees of freedom are frozen. Moreover, the position of T_{gap} with respect to T_c gives a better understanding of the transition. In the RNA case where $T_c < T_{\text{gap}}$, the interpretation is that there exists frozen pairs in the high-temperature phase, but only of finite size [14]. Here, in the directed polymer case where $T_{\text{gap}} < T_c$, there exists frozen monomers only below T_{gap} , whereas for $T_{\text{gap}} < T < T_c$, the localization occurs on a tube of finite extent $\xi(T)$.

-
- [1] M. Mezard, G. Parisi and M. A. Virasoro, 'Spin Glass Theory and beyond', World Scientific, Singapore, (1987).
 - [2] B. Derrida, Phys. Rev. B 24, 2613 (1981); B. Derrida and G. Toulouse, J. Phys. Lett. (France), 46, L223 (1985).
 - [3] B. Derrida and H. Spohn, J. Stat. Phys., 51, 817 (1988).
 - [4] B. Derrida, 'Non-self-averaging effects in sums of random variables, spin glasses, random maps and random walks', in 'On three levels' Eds M. Fannes et al (1994) New-York Plenum Press.
 - [5] B. Derrida and H. Flyvbjerg, J. Phys. A Math. Gen. 20, 5273 (1987).
 - [6] P. L. Krapivsky, I. Grosse and E. Ben-Naim, Phys. Rev. E 61, R993 (2000).
 - [7] P. G. Higgs, Phys. Rev., E 51, 95 (1995).
 - [8] B. Derrida and B. Jung-Müller, J. Stat. Phys. 94, 277 (1999).
 - [9] B. Derrida, Spin glasses, random Boolean networks and simple models of evolution, Proceedings of the Trieste Conference on Nonlinear cooperative phenomena in biological systems, August 1997, p 216-226 in Non linear cooperative phenomena in biological systems Ed L. Mattsson, World Scientific (1998).
 - [10] L. Frachebourg, I. Ispolatov and P. L. Krapivsky, Phys. Rev. E 52, R5727 (1995).
 - [11] D. Ertas and Y. Kantor, Phys. Rev. E 53, 846 (1996); S. Wolking and Y. Kantor, EPJB 12, 569 (1999).
 - [12] B. Derrida, R. B. Griffiths and P. G. Higgs, Europhys. Lett, 18, 361 (1992).
 - [13] S. R. Morgan and P. G. Higgs, J. Phys A 31, 3153 (1998).
 - [14] C. Monthus and T. Garel, cond-mat/0611611, to appear in Phys. Rev. E.
 - [15] T. Halpin-Healy and Y.-C. Zhang, Phys. Repts., 254, 215 (1995).
 - [16] C. Monthus and T. Garel, cond-mat/0701699.
 - [17] P. Camona and Y. Hu, Prob. Th. and Rel. Fields 124, 431 (2002); P. Camona and Y. Hu, math.PR/0601670.
 - [18] F. Comets, T. Shiga and N. Yoshida, Bernoulli 9, no. 4, 705 (2003).
 - [19] V. Vargas, math.PR/0603233.
 - [20] M. Mezard, J. Phys. (France), 51, 1831 (1990).
 - [21] D. S. Fisher and D. A. Huse, Phys. Rev. B 43, 10728 (1991).
 - [22] T. Hwa and D. S. Fisher, Phys. Rev. B 49, 3136 (1994).
 - [23] D. S. Fisher and D. A. Huse, Phys. Rev. B 38, 386 (1988).
 - [24] J. Z. Imbrie and T. Spencer, J. Stat. Phys. 52, 609 (1988).
 - [25] J. Cook and B. Derrida, J. Stat. Phys. 57, 89 (1989).
 - [26] D. A. Huse, C. L. Henley, and D. S. Fisher, Phys. Rev. Lett. 55, 2924 (1985).
 - [27] M. Kardar, Nucl. Phys. B 290, 582 (1987).
 - [28] K. Johansson, Comm. Math. Phys. 209, 437 (2000).
 - [29] M. P. Radofer and H. Spohn, Physica A 279, 342 (2000); M. P. Radofer and H. Spohn, Phys. Rev. Lett. 84, 4882 (2000); M. P. Radofer and H. Spohn, J. Stat. Phys. 108, 1071 (2002); M. P. Radofer and H. Spohn, J. Stat. Phys. 115, 255 (2002).
 - [30] E. M. Arinari, A. Pagnani and G. Parisi, J. Phys. A 33, 8181 (2000); E. M. Arinari, A. Pagnani and G. Parisi and Z. Racz, Phys. Rev. E 65, 026136 (2002).
 - [31] C. Monthus and T. Garel, Phys. Rev E 73, 056106 (2006).